Calculation of metallic and insulating phases of V2O3 by hybrid density functionals

Yuzheng Guo, Stewart J. Clark, and John Robertson

Citation: The Journal of Chemical Physics **140**, 054702 (2014); doi: 10.1063/1.4863325
View online: http://dx.doi.org/10.1063/1.4863325
View Table of Contents: http://scitation.aip.org/content/aip/journal/jcp/140/5?ver=pdfcov
Published by the AIP Publishing

Calculation of metallic and insulating phases of V_2O_3 by hybrid density functionals

Yuzheng Guo,[1] Stewart J. Clark,[2] and John Robertson[1,a)]
[1]*Department of Engineering, University of Cambridge, Cambridge CB3 0FA, United Kingdom*
[2]*Department of Physics, University of Durham, Durham DH1 3LE, United Kingdom*

(Received 8 October 2013; accepted 14 January 2014; published online 3 February 2014)

The electronic structure of vanadium sesquioxide V_2O_3 in its different phases has been calculated using the screened exchange hybrid density functional. The hybrid functional accurately reproduces the experimental electronic properties of all three phases, the paramagnetic metal (PM) phase, the anti-ferromagnetic insulating phase, and the Cr-doped paramagnetic insulating (PI) phase. We find that a fully relaxed supercell model of the Cr-doped PI phase based on the corundum structure has a monoclinic-like local strain around the substitutional Cr atoms. This is found to drive the PI-PM transition, consistent with a Peierls-Mott transition. The PI phase has a calculated band gap of 0.15 eV, in good agreement with experiment. © *2014 AIP Publishing LLC*. [http://dx.doi.org/10.1063/1.4863325]

I. INTRODUCTION

The vanadium oxides have been extensively studied as canonical examples of metal insulator transitions (MIT) in a correlated oxide system which can be accessed by varying the temperature, pressure, or doping.[1,2] In particular, V_2O_3 exhibits three phases, a paramagnetic metallic (PM) phase with the corundum structure, a paramagnetic insulating (PI) phase with the same corundum structure, accessed by Cr doping or pressure, and a monoclinic antiferromagnetic insulator (AFI) phase which is stabilized at low temperature, Fig. 1. Early approaches used crystal field theory to account for the level splitting of the V 3*d* states, the orbital occupancies and the spin states.[3] Later, X-ray photoemission spectra (XPS), X-ray absorption spectra (XAS), and the optical response[4–15] were used to understand the changes of electronic structure across the transitions.

At the same time, electronic structure calculations of increasing sophistication have been employed to treat V_2O_3.[16–26] The simple local spin density approximation (LSDA) is known to be unable to give a band gap for the insulating phases of V_2O_3[16] due to its inability to treat the localized *d* electrons correctly. On the other hand, the LSDA+U method can open up a gap for open-shell d electron systems,[17] but with the disadvantage that the on-site repulsion, U, is a variable. Thus, more sophisticated calculation methods such as the GW method[18] are used, which can give a gap in the AFI phase of V_2O_3. The dynamic mean field theory (DMFT) also finds a band gap in both the AFI and PI phases.[19–23] The aim of GW and DMFT is to give the best description of the electronic structure of a few (embedded) atoms. However, both GW and DMFT require a previous local density calculation to determine the equilibrium geometry. There is no simultaneous calculation of the atomic and electronic structure. However, in Peierls transitions or at defects, the electronic structure depends directly on the atomic structure, so it is desirable to have a calculation method that gives the atomic and electronic structures in a "single shot." In addition, GW and DMFT are computationally expensive, and lower cost methods are desirable.

The need for single shot methods arises from two causes. First, there has always been an interest in whether a specific system was a Mott insulator or a Peierls insulator, such as in vanadates and manganites and many related oxide systems.[27–29] However, it is not so easy to follow the electronic structure across a transition where the atomic structure varies. Second, there is growing interest in using correlated oxide systems such as vanadium oxides in microelectronics, such as in high switching current Mott field effect transistors or "Mott-FETs,"[30–32] in non-volatile resistive random access memories (RRAM),[33] and in fast optical switches.[34–39] Peierls-based RRAMs can have fast switching speeds arise because a Peierls transition involves small atomic displacements, compared to the longer distance migration of oxygen vacancies that occurs in a conventional RRAMs.

The modeling of such systems and applications for correlated oxides would benefit from having a lower cost variational method that would predict the band gap and atomic geometry, using ~100 atom supercell models of doped, defective, or disordered oxide systems. We show that hybrid functionals could provide such an approach for V_2O_3.

Hybrid density functionals are family of orbital-dependent exchange-correlation functionals where a fraction of Hartree-Fock (HF) exchange is mixed into the local exchange-correlation density functional of density functional theory.[40–49] Several hybrid functionals have been developed, such as the B3LYP,[41] PBE0, the Heyd, Scuseria, Ernzerhof (HSE) methods,[42,43] and screened exchange (sX)[40,48,49] method. Hybrid functionals are generalised Kohn-Sham functionals,[42] so they can be used variationally to relax geometries, give good band gaps,[46–49] and are efficient enough to treat supercells of 100 or more atoms. Hybrid functionals

a)jr@eng.cam.ac.uk

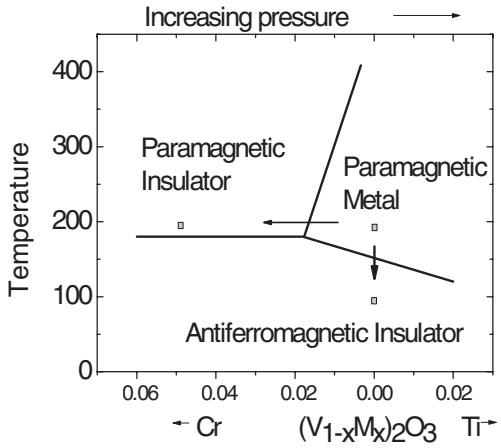

FIG. 1. Schematic magnetic phase diagram of V_2O_3 with respect to Cr (and Ti) doping.

have been used to calculate the single particle band structures of various transition metal oxides.[50–54] The HSE functional was used previously to study the MIT in VO_2 with changing the crystal structure,[50] but based on experimental atomic coordinates. Here, we find that the sX functional will reproduce the correct single-particle electronic structure in all the three phases of V_2O_3 without any fitting parameter. This validates the observation of Iori *et al.*[45] that the failure of LSDA to treat these correlated electron systems is due to its poor description of the exchange interaction, not the correlation.

We noted above that GW and DMFT could provide good descriptions of the electronic structures of each phase. It was initially thought that pressure and doping had the same effect on the MIT.[2] To date, DMFT studies tended to use the experimental contraction of the lattice parameters and the internal atomic coordinates of a pure PM V_2O_3 primitive cell to simulate Cr doping.[21,22] However, recent experiments show that the PI-PM transition due to pressure and Cr doping are not equivalent.[7] A supercell calculation is highly desired by the DMFT community. Thus, Cr doping must be allowed to vary the internal atomic positions. Here, we present a one-shot study of the Cr-doped V_2O_3 PI phase with local atomic relaxations, by substituting Cr atoms in a large V_2O_3 supercell and relaxing internal geometries variationally using the sX hybrid functional. Note that the ground state of V_2O_3 is antiferromagnetic not non-magnetic, so the possible problem[55] noted for HSE in VO_2 does not apply.

II. METHOD

The calculations are carried out with the CASTEP plane-wave pseudopotential code.[56] Norm-conserving pseudopotentials were generated by the OPIUM code.[57] The plane wave cutoff energy is set to 780 eV with a total energy convergence of better than 0.01 eV per atom. For primitive cells, the Brillouin zone integrations use a $4 \times 4 \times 4$ Monkhorst-Pack (MP) grid giving a similar level of convergence. An MP grid of $5 \times 5 \times 5$ is used to calculate the density of states (DOS).

Fig. 2 shows the corundum R3c structure in the primitive cell and the 120-atom supercell model of the Cr-doped

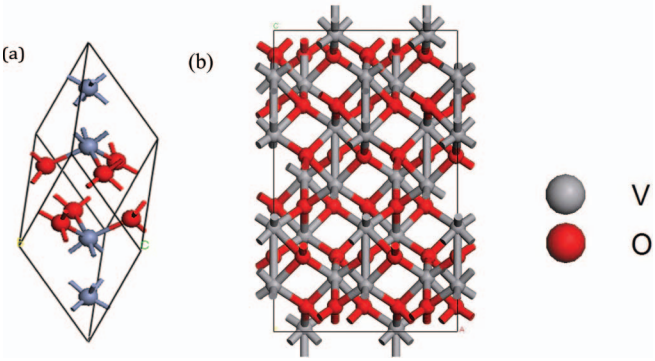

FIG. 2. (a) Corundum structure primitive cell. Oxygen = red, V = grey. (b) Supercell used to calculate the doped PI phase.

V_2O_3 PI phase. The supercell consists of a $2 \times 2 \times 1$ supercell of the hexagonal corundum unit cell and it has 2 Cr atoms, equivalent to 4.2% of Cr. Two Cr atoms per supercell are needed to model the PI phase, as a single spin from one Cr atom will transform the whole system into an AFI phase. The internal coordinates of the supercell are completely relaxed with spin-degenerate sX functional. The residual force is less than 0.01 eV/A. Only the Γ point is used for the geometry relaxation. A $3 \times 3 \times 1$ MP grid is used for the DOS calculation for this supercell.

III. RESULTS

In the corundum structure (Fig. 2(a)), the V atoms are surrounded by an octahedron of oxygen atoms with a trigonal distortion, which splits the 3*d* states into singly degenerate a_{1g} and doubly degenerated e_{2g} states. It was shown both by experiment and calculation that V has a mixed orbital occupation where both a_{1g} and e_{2g} states are partially filled.[6,17,21,22] In the monoclinic structure, the adjacent V atoms form weak V–V bonds in the plane perpendicular to the z axis.

Fig. 3 shows the band structure and partial density of states (PDOS) of the PM phase using the experimental hexagonal cell lattice constants (a = 4.951 Å and c = 14.004 Å). The Fermi level E_F is set to 0 eV and lies within the V $3d\pi$ states. The V $3d\pi$ states above −1 eV hybridize weakly with O *p* states. The O 2*p* states lie from −4 eV to −8 eV and hybridize significantly with V $d\sigma$ states. The V 3*d* band above −1 eV is noticeably narrower in the PM than in the other phases. The lowest band at −0.8 eV has a sizable dispersion along Γ-L-M representing the a_{1g} bonding state of the V–V pair (Fig. 3(b)).

Fig. 4 compares the calculated DOS with that from photoemission.[6,10] Table I compares the various band widths and the energies of peaks A and B in the V 3*d* valence band as calculated by different methods and from photoemission.[6,10] The peaks A and B are labeled in Fig. 4. We find that the total DOS of the PM phase in sX is similar to that found by DMFT.[21] The O 2*p* states are shifted down by 1 eV in sX compared to in LDA, and the V 3*d* valence band is wider in sX and DMFT[19] than in LDA, consistent with the photoemission spectra.[5,6,10] Some V *s* character is found at −8 eV in Fig. 3(a), as seen in previous calculations.[10]

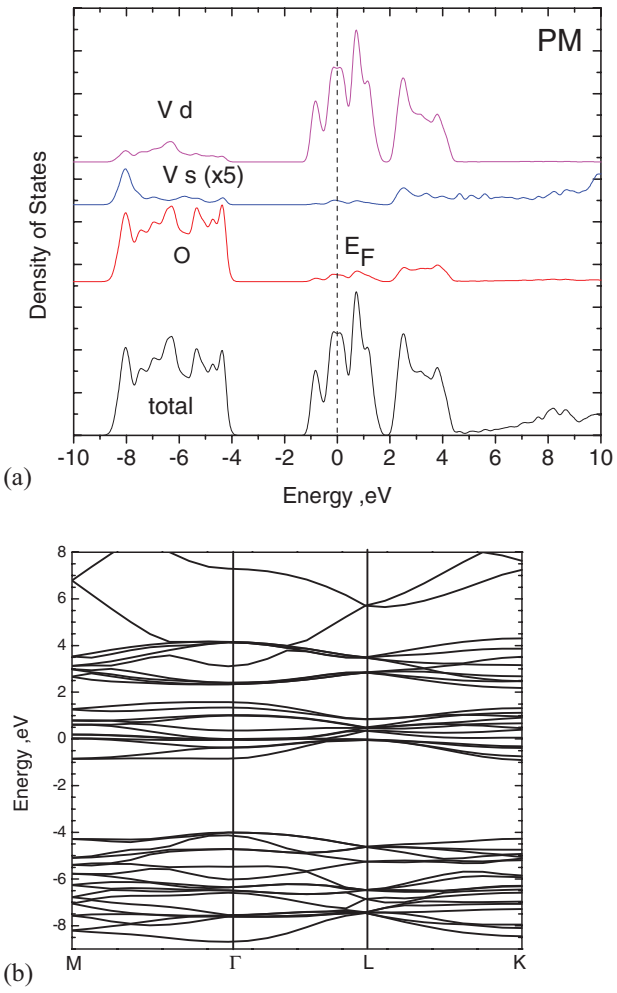

FIG. 3. (a) Calculated total and partial DOS for PM phase. (b) The band structure of PM phase in the hexagonal version of the unit cell. The Fermi level is at 0 eV.

TABLE I. Comparison of the calculated DOS to XPS data. The two peaks in the V 3*d* PDOS are labeled in Fig. 4.

	eV	VB width	V 3*d* width	Peak A	Peak B
PM	Expt.[6,11]	9.2	1.5	0.2	1.4
	PBE[16]	8.2	1	0.1	0.9
	DMFT[21,22]	...	1.5	0.2	1.4
	sX	8.8	1.2	0.1	1
AFI	Expt.[6,17]	9.2	2.2	0.5	1.2
	LDA+U[18]	...	1.2	0.4	1
	sX	8.8	1.9	0.4	1.0–1.4
PI	Expt.[6,11]	9.2	2.2	0.5	1.1
	PBE[16]	8.2	1	0.1	0.9
	U+GW[18]	8.6	1	0.1	0.9
	DMFT[21,22]	...	2.2	0.1	1.2
	sX	8.8	2.2	0.4	1.1–1.5

Fig. 5 shows the bands and PDOS for the AFI phase in sX. The VBM is set to 0 eV. The O 2*p* states are still separated from the V 3*d* states, but the V 3*d*-O 2*p* hybridization is stronger here than in the PM phase. Both the valence band maximum (VBM) and the conduction band minimum (CBM) consist of V 3*d* states, consistent with a Mott-Hubbard insulator. The O 2*p* and V 3*d* valence bands are both wider than in the PM phase (Fig. 4, Table I). A sharp peak in the valence band at −0.8 eV in the PM phase disappears and is replaced by several peaks from 0 to −1.5 eV, consistent with photoemission for the AFI phase.[6,12] A high resolution hard X-ray photoemission spectrum confirms that the valence band spectrum has many components[6] with two large

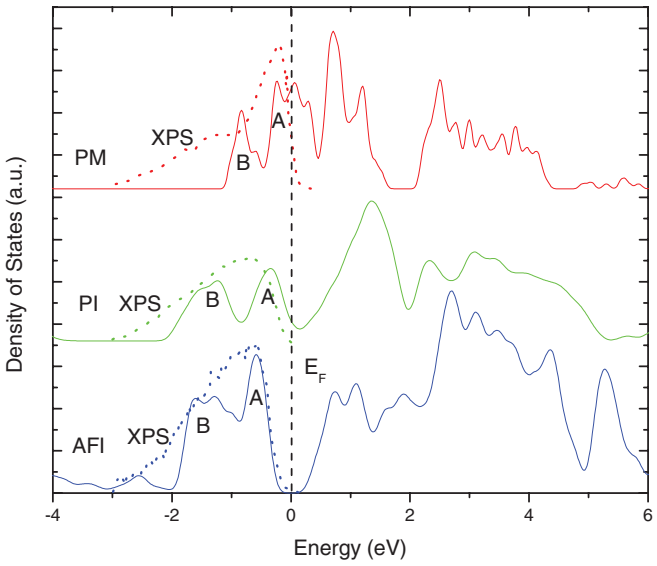

FIG. 4. Total DOS of each phase compared to photoemission spectra.[6] Here, the Fermi energy of the PM phase is set to 0 eV, and the midgap of the AFI and PI phases is set to 0 eV.

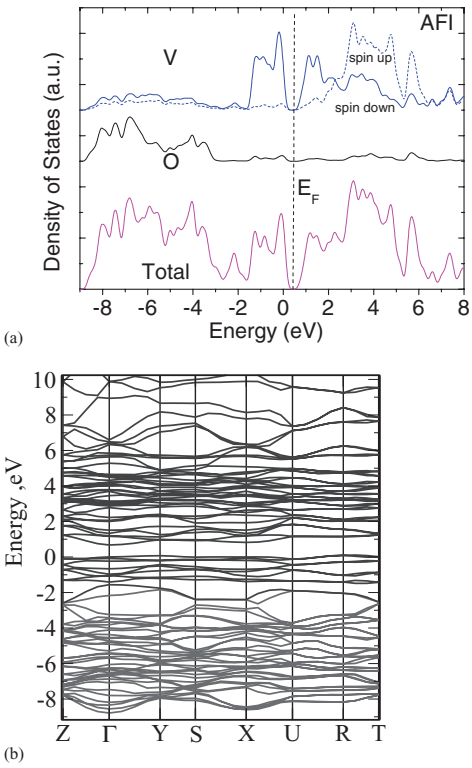

FIG. 5. (a) The DOS and partial DOS of monoclinic AFI phase. (b) The band structure of monoclinic AFI phase. VBM is set to 0 eV.

TABLE II. Comparison of experimental band gaps and those calculated by different functionals for the AFI phase.

	Optical gap[61–63]	LDA[16]	LDA+U[17]	GW[18]	U+GW[18]	sX
E_g(direct) (eV)	0.5–0.66	0	0.60	0	0.943	0.76
E_g(indirect) (eV)					0.835	0.63

peaks labeled A and B lying at −0.3 eV and −1.1 eV, respectively. Our DOS has two large peaks at −0.1 eV and −1.2 eV. LDA+DMFT does not reproduce the peak A.[19,21,22] The magnetic moment of the V atom is calculated to be 1.8 μ_B, close to the LDA+U value[17] of 1.7 μ_B. The spin is automatically relaxed in the spin-polarized calculation, thus this value identifies the S = 1 local moment as the ground state, consistent with experiment[58] and previous analysis,[59,17] and contrary to the Castellini model.[60]

Fig 5(b) shows the band structure of the AFI phase. The calculated band gap of 0.63 eV agrees well with the experimental optical gap of 0.50–0.66 eV.[51,54–56] AFI V_2O_3 has an indirect gap with a VBM between R and T, and a CBM at Γ. The direct gap at Γ is 0.1 eV wider than the indirect gap. The band gaps from different calculations and experiments are compared in Table II. Our results are similar to the band structure from the U+GWA method[18] but the band gap is more accurate and covers more of reciprocal space.

Turning to the PI phase, the corundum structure without doping gives a metallic ground state and the monoclinic structure gives an insulating ground state in sX. For the supercell model of the PI phase, the internal coordinates are relaxed within sX. The Cr atom, surrounded by an oxygen octahedron, has the same local symmetry as V, but individual bond lengths now change. Due to the limit on supercell size, we studied the MIT at the Cr content of 4.2% not the experimental value of ∼1.5%. We find that at 4.2% Cr *c* increases by 1.3% and *a* decreases by 0.5%, consistent with experimental lattice parameter data.[6,8]

Fig. 6 shows the total DOS, PDOS, and bands of a PI V_2O_3 cell with 4.2% Cr doping. The V 3*d* valence PDOS resembles that of the AFI phase. The V 3*d* states range from 0 eV to −2 eV, almost twice as wide as in the PM phase. The multi-peak feature remains, with two prominent PDOS peaks at a similar energy as in AFI phase. The calculated band gap of 0.16 eV in Fig. 6(b) is consistent with the photoemission value of 0.1 eV.[6,10] The VBM is localized around Cr atoms while the CBM consists of one flat band delocalized on V atoms. There is a similar band of 0.19 eV separating the CBM from the bulk conduction bands. We also plot in Fig. 6 the partial DOS of Cr and V. The Cr PDOS is similar to that of V. The states from V and Cr are highly hybridized. The most significant peak from the Cr PDOS is about −1.8 eV from the Fermi level, in good agreement with the small peak at −2 eV seen by Mo *et al.*[6] The highly localized band edges from V 3*d* states suggest the PI phase to be a typical Mott-Hubbard type.

We do not expect sX to fully match the photoemission spectra because the dynamical effects included in DMFT are not present. But the band gap opening in different phases of V_2O_3 shows that the band structures of strongly correlated

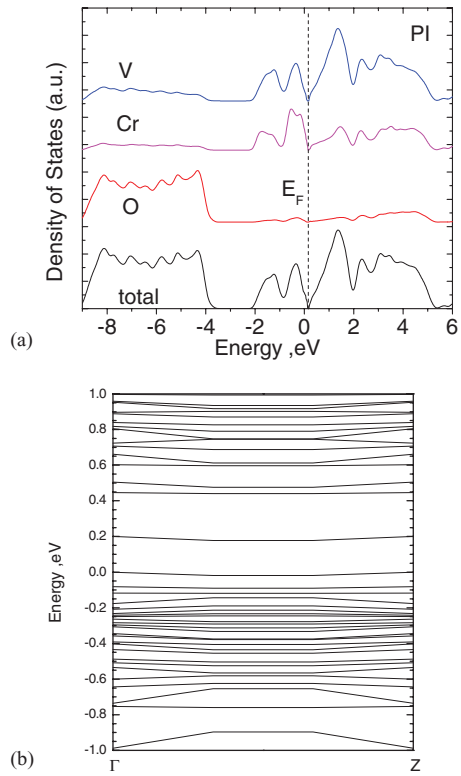

FIG. 6. (a) The total and partial DOS of the corundum PI phase. (b) Band structure of PI phase near the band gap.

electrons are greatly improved over (semi-) local functionals by introducing the non-local exchange. sX provides a reasonable description of single particle states in strongly correlated systems at an affordable computational cost. Advanced methods such as DMFT and GW corrections can be applied on top of sX if necessary to include dynamic effects.

The metal-oxygen bond lengths in the PI phase are summarized in Table III. The average bond length in the PI phase is the same as in PM. However, the average Cr–O bond length of 2.07 Å is 2% larger than the V–O bond length of 2.02 Å. The metal-metal distances change more significantly. The in-plane metal-metal bonds shrink by 24% from 2.97 Å to 2.24 Å. The shortened metal-metal bonds in PI resemble the bonding in the AFI phase (Fig. 7). Therefore, Cr-doping introduces significant local strain.[14]

We have stretched the primitive cell of corundum PM phase in different modes including uniaxial, biaxial, and uniform tension. None of these macroscopic strain modes can alone induce the MIT. Fig. 7 compares the atomic local structures of each phase. Fig. 7(a) shows the corundum structure

TABLE III. Comparison of calculated metal-oxygen bond lengths in each phase.

	PM corundum	AFI monoclinic	PI corundum
Metal-O bond length (Å)	2.02	1.94	2.02(V–O)
			2.07(Cr–O)
Metal-metal bond (Å)	2.78	2.87	2.81(V–V)
			2.72(Cr–V)

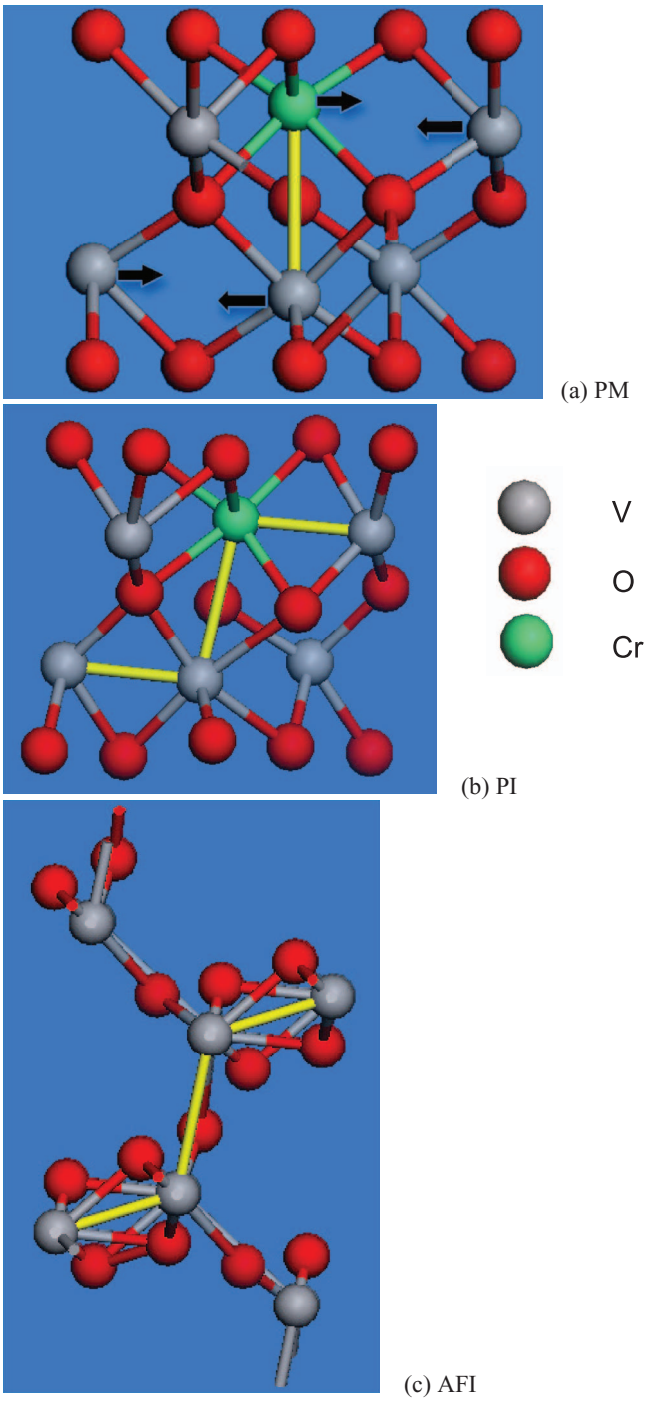

FIG. 7. Calculated local atomic structure of PM (a), PI(b), and AFI(c) phases. Oxygen = red ,V = grey. The doped Cr atom is shown as green. The yellow bond in (a) is the metal-metal pair bonding along diagonal in corundum structure (2.78 Å). The arrows show the deviation of V atoms induced by Cr doping. The planar distance between metals is 2.97 Å and thus is not shown as bond. (b) and (c) The more planar yellow bonds are formed between the neighboring metal atoms in the xy plane perpendicular to the diagonal in corundum structure. (b) The planar bond length is 2.24 Å while Cr–V is 2.72 Å. (c) The planar bond length is 2.39 Å while the diagonal one is 2.89 Å.

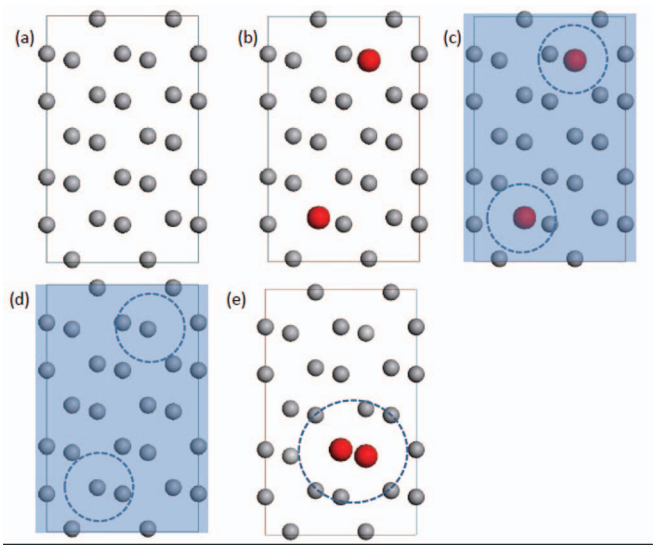

FIG. 8. (a) Perfect cell; (b) Cr doped cell with no relaxation; (c) Cr doped relaxed cell; (d) relaxed doped cell but without doping; and (e) Cr-dimer doped fully relaxed cell. Only V and Cr atoms are shown. V = grey, dopant Cr = red. Insulating phases shown shaded. *Note the correlation of insulating to relaxed cell with separated dopants.*

without relaxation. Only metal atoms along the diagonal are paired, as shown by the yellow bond. Fig. 7(b) shows the relaxed PI structure. The Cr tends to bond with the planar neighboring V's. The Cr–V bonding in the xy plane shifts the metal atom towards the hollow site in the corundum structure as shown by the arrows in Fig. 7(a). The original metal dimer along the c axis is thus tilted. If the Cr concentration is low, only the local atomic structure is affected and there is no long-range structural change. If the distance between neighboring Cr atoms is small enough, all the metal atoms will deviate from corundum structure and form a zigzag chain. The oxygen octahedron has been retained. In the monoclinic AFI structure, the metal atoms have been further displaced and the oxygen octahedra have also been severely distorted. If we compare the metal bonding, it is clear that the PI and AFI phases share similar metal-metal bonds as shown by the yellow lines. As both band edges in all phases are mainly metal *d* type, the PI phase with similar metal distortion has the similar valence band width as the AFI phase.

The key question is whether electron doping or structural (Peierls) distortion drives the PI-PM MIT. In order to separate these two effects, we calculated the band structure of unrelaxed Cr-doped V_2O_3 and the relaxed geometry without doping, using the same 120-atom supercells, as shown schematically in Fig. 8. Insulating supercells are shown shaded. The relaxed "undoped" cell is achieved by back-substituting V for Cr into the relaxed cell. The unrelaxed system remains metallic. The relaxed cell with no doping is insulating, with a similar band gap to the doped sample. Combined with the previous Cr PDOS analysis, we therefore argue that local strain rather than doping causes this MIT. If local strain is the driving force for the transition, this will depend on dopant positions. If the two Cr atoms are far away from each other as above, the supercell is found to be insulating. However, if the two Cr atoms are close together as a dimer, Fig. 8(e), the effective strain is less and the cell remains metallic. The Cr-dimer doped V_2O_3 further confirms that electron doping is not the main driving force. Overall, the extra two electrons of two Cr atoms enter an extra valence state, and the MIT works by a strain opening of the band gap. Thus, our calculations suggest that the PM-PI

transition of V_2O_3 has a component of Peierls transition in it, to add to its Mott-like character, like in VO_2,[28] driven by V–V chain formation. Whereas it has been noted that V^{4+} oxides are generally Peierls insulators and V^{3+} oxides are generally Mott insulators,[27] the contribution of lattice relaxation to the band gap opening in PI V_2O_3 suggests that V_2O_3 is also a Peierls-Mott system.

Overall, Fig. 4 and Tables I and II show that the sX method gives spectroscopic features in good agreement with experiment. The band gaps and band widths are good. The peak positions in the upper valence band found by sX compare to within 0.1 eV of experiment and comparable to those found by DMFT or GW.

IV. CONCLUSIONS

In summary, we have calculated the electronic structure of the PM, PI, and AFI phases of V_2O_3 with the sX hybrid functional. The PI phase is simulated by 4.2% Cr doping in a supercell, and the internal atomic coordinates are relaxed with sX. The sX functional with local relaxations gives correctly the metallic and both insulating phases. A calculation of unrelaxed and un-doped V_2O_3 supercells shows that local distortions around Cr sites rather than electron doping is the main driving force for the PM/PI MIT. The band gaps of the PI and AFI phases are 0.15 eV and 0.63 eV, in good agreement with experiment. The band widths are also in good agreement with photoemission. Overall, this suggests that hybrid functionals provide a simple, single-shot method to analyze complex metal insulator transitions combining Peierls and Mott-like components. It emphasizes that it is improvements to the LSDA description of the exchange interaction not the correlation interactions that are needed to correctly describe oxides with correlate *d* states.

[1] M. Imada, A. Fujimori, and Y. Tokura, Rev. Mod. Phys. **70**, 1039 (1998).
[2] D. B. McWhan and J. P. Remeika, Phys. Rev. B **2**, 3734 (1970).
[3] J. B. Goodenough, Prog. Solid State Chem. **5**, 145 (1971); J. B. Goodenough and J. S. Zhou, Chem. Mater. **10**, 2980 (1998).
[4] K. E. Smith and V. E. Henrich, Phys. Rev. B **38**, 5965 (1988).
[5] R. Zimmermann, P. Steiner, R. Claessen, F. Reinert, S. Hufner, P. Blaha, and P. Dufek, J. Phys. Condens. Matter **11**, 1657 (1999).
[6] S. K. Mo, H. D. Kim, J. D. Denlinger, J. W. Allen, J. H. Park, A. Sekiyama, A. Yamasaki, S. Suga, Y. Saitoh, T. Muro, and P. Metcalf, Phys. Rev. B **74**, 165101 (2006).
[7] F. Rodolakis, P. Hansmann, J. P. Rueff, A. Toschi, M. W. Haverkort, G. Sangiovanni, A. Tanaka, T. Saha-Dasgupta, O. K. Andersen, K. Held, M. Sikora, I. Alliot, J. P. Itiè, F. Baudelet, P. Wzietek, P. Metcalf, and M. Marsi, Phys. Rev. Lett. **104**, 047401 (2010).
[8] F. Rodolakis, J. P. Rueff, M. Sikora, I. Alliot, J. P. Itiè, F. Baudelet, S. Ravy, P. Wzietek, P. Hansmann, A. Toschi, M. W. Haverkort, G. Sangiovanni, K. Held, P. Metcalf, and M. Marsi, Phys. Rev. B **84**, 245113 (2011).
[9] F. Rodolakis, B. Mansart, E. Papalazarou, S. Gorovikov, P. Vilmercati, L. Petaccia, A. Goldini, J. P. Rueff, S. Luipi, P. Metcalf, and M. Marsi, Phys. Rev. Lett. **102**, 066805 (2009).
[10] E. Papalazarou, M. Gatti, M. Marsi, V. Brouet, F. Iori, L. Reining, E. Annese, I. Vobornik, F. Offi, A. Fondacaro, S. Huotari, P. Lacovig, O. Tjemberg, N. B. Brookes, M. Sacchi, P. Metcalf, and G. Pannaccioni, Phys. Rev. B **80**, 155115 (2009).
[11] H. Fujiwara, A. Sekiyama, S. K. Mo, J. W. Allen, J. Yamaguchi, G. Funabashi, S. Imada, P. Metcalf, A. Higashiya, M. Yabashi, K. Tamasaku, T. Ishikawa, and S. Suga, Phys. Rev. B **84**, 075117 (2011).
[12] S. Lupi, L. Baldassarre, B. Mansart, A. Perucchi, A. Barinov, P. Dudin, E. Papalazarou, F. Rodolakis, J. P. Rueff, J. P. Itiè, S. Ravy, D. Nicoletti, P. Postorino, P. Hansmann, N. Parragh, A. Toschi, T. Saha-Dasgupta, O. K. Andersen, G. Sangiovanni, K. Held, and M. Marsi, Nat. Commun. **1**, 105 (2010).
[13] B. Mansart, A. Barinov, P. Dudin, L. Baldassarre, E. Papalazarou, P. Metcalf, S. Lupi, and M. Marsi, Appl. Phys. Lett. **100**, 014108 (2012).
[14] A. I. Frenkel, D. M. Pease, J. I. Budnick, P. Metcalf, E. A. Stern, P. Shanthakumar, and T. Huang, Phys. Rev. Lett. **97**, 195502 (2006).
[15] A. Perucchi, L. Baldassarre, B. Postorino, and S. Lupi, J. Phys. Condens. Matter **21**, 323202 (2009).
[16] L. F. Mattheiss, J. Phys.: Condens. Matter **6**, 6477 (1994).
[17] S. Y. Ezhov, V. I. Anisimov, D. I. Khomskii, and G. A. Sawatzky, Phys. Rev. Lett. **83**, 4136 (1999).
[18] S. Kobayashi, Y. Nohara, S. Yamamoto, and T. Fujiwara, Phys. Rev. B **78**, 155112 (2008).
[19] A. I. Poteryaev, J. M. Tomczak, S. Biermann, A. Georges, A. I. Lichtenstein, A. N. Rubtsov, T. Saha-Dasgupta, and O. K. Andersen, Phys. Rev. B **76**, 085127 (2007).
[20] A. Georges, G. Kotliar, W. Krauth, and M. J. Rozenberg, Rev. Mod. Phys. **68**, 13 (1996).
[21] K. Held, G. Keller, V. Eyert, D. Vollhardt, and V. I. Anisimov, Phys. Rev. Lett. **86**, 5345 (2001).
[22] G. Keller, K. Held, V. Eyert, D. Vollhardt, and V. I. Anisimov, Phys. Rev. B **70**, 205116 (2004).
[23] R. J. O. Mossanek, M. Abbate, T. Yoshida, A. Fujimori, Y. Yoshida, N. Shirkawa, H. Eisaki, S. Kohno, and F. C. Vicentini, Phys. Rev. B **78**, 075103 (2008).
[24] J. C. Woicik, M. Yekutiel, E. J. Nelson, N. Jacobson, P. Pfalzer, M. Klemm, S. Horn, and L. Kronik, Phys. Rev. B **76**, 165101 (2007).
[25] F. Iori, F. Rodolakis, M. Gatti, L. Reining, M. Upton, Y. Shvydko, J. P. Rueff, and M. Marsi, Phys. Rev. B **86**, 205132 (2012).
[26] D. Grieger, C. Piefke, O. E. Peil, and F. Lechermann, Phys. Rev. B **86**, 155121 (2012).
[27] Y. Ishige, T. Sudayama, Y. Wakisaka, T. Mizokawa, H. Wadati, G. A. Sawatzky, T. Z. Regier, M. Isobe, and Y. Ueda, Phys. Rev. B **83**, 125112 (2011).
[28] C. Weber, D. D. O'Regan, N. D. M. Hine, M. C. Payne, G. Kotliar, and P. B. Littlewood, Phys. Rev. Lett. **108**, 256402 (2012).
[29] D. I. Khomskii, J. Mag. Mag. Mater. **306**, 1 (2006).
[30] J. Son, S. Rajan, S. Stemmer, and S. J. Allen, J. Appl. Phys. **110**, 084503 (2011).
[31] M. Boucherit, O. F. Shoron, T. A. Cain, C. A. Jackson, S. Stemmer, and S. Rajan, Appl. Phys. Lett. **102**, 242909 (2013).
[32] P. Moetakef, T. A. Cain, D. G. Ouellette, J. Y. Zhang, D. O. Klenov, A. Janotti, C. G. van de Walle, S. Rajan, S. J. Allen, and S. Stemmer, Appl. Phys. Lett. **99**, 232116 (2011).
[33] K. Martens, I. P. Radu, S. Mertens, X. Shi, and L. Nyns, J. Appl. Phys. **112**, 124501 (2012).
[34] A. Cavalleri *et al.*, Phys. Rev. Lett. **87**, 237401 (2001); Phys. Rev. B **70**, 161102 (2004).
[35] H. T. Kim *et al.*, Phys. Rev. Lett. **97**, 266401 (2006).
[36] C. Kubler *et al.*, Phys. Rev. Lett. **99**, 116401 (2007).
[37] P. Baum, D. S. Yang, and A. H. Zewail, Science **318**, 788 (2007).
[38] J. Nag, R. F. Haglund, E. A. Payant, and K. L. More, J. Appl. Phys. **112**, 103532 (2012).
[39] X. Yuan, W. Zhang, and P. Zhang, Phys. Rev. B **88**, 035119 (2013).
[40] D. M. Bylander and L. Kleinman, Phys. Rev. B **41**, 7868 (1990).
[41] A. D. Becke, J. Chem. Phys. **98**, 1372 (1993).
[42] A. Seidl, A. Görling, P. Vogl, J. A. Majewski, and M. Levy, Phys. Rev. B **53**, 3764 (1996).
[43] J. Heyd, G. E. Scuseria, and M. Ernzerhof, J. Chem. Phys. **118**, 8207 (2003).
[44] A. V. Krukau, O. A. Vydropv, A. F. Izmaylov, and G. E. Scuseria, J. Chem. Phys. **125**, 224106 (2006).
[45] J. Paier, M. Marsman, K. Hummer, G. Kresse, I. C. Gerber, and J. G. Angyan, J. Chem. Phys. **124**, 154709 (2006).
[46] M. Marsman, J. Paier, A. Stropa, and G. Kresse, J. Phys. Condens. Matter **20**, 064201 (2008).
[47] J. Muscat, A. Wander, and N. M. Harrison, Chem. Phys. Lett. **342**, 397 (2001).
[48] K. Xiong, J. Robertson, M. C. Gibson, and S. J. Clark, Appl. Phys. Lett. **87**, 183505 (2005).
[49] S. J. Clark and J. Robertson, Phys. Rev. B **82**, 085208 (2010).
[50] V. Eyert, Phys. Rev. Lett. **107**, 016401 (2011).

[51]F. Iori, M. Gatti, and A. Rubio, Phys. Rev. B **85**, 115129 (2012).
[52]C. Rodl, F. Fuchs, J. Furthmuller, and F. Bechstedt, Phys. Rev. B **79**, 235114 (2009).
[53]Y. Guo, S. J. Clark, and J. Robertson, J. Phys.: Condens. Matter **24**, 325504 (2012).
[54]R. Gillen and J. Robertson, Phys. Rev. B **87**, 125116 (2013).
[55]R. Grau-Crespo, H. Wang, and U. Schwingenschlogl, Phys. Rev. B **86**, 081101 (2012).
[56]M. D. Segall, P. J. D. Lindan, M. J. Probert, C. J. Pickard, P. J. Hasnip, S. J. Clark, and M. C. Payne, J. Phys. Condens. Mater. **14**, 2717 (2002); S. J. Clark, M. D. Segall, C. J. Pickard, P. J. Hasnip, M. J. Probert, K. Refson, and M. C. Payne, Zeit. Krist. **220**, 567 (2005).
[57]A. M. Rappe, K. M. Rabe, E. Kaxiras, and J. D. Joannopoulos, Phys. Rev. B **41**, 1227 (1990).
[58]G. A. Thomas, D. H. Rapkine, S. A. Carter, A. J. Millis, T. F. Rosenbaum, P. Metcalf, and J. M. Honig, Phys. Rev. Lett. **73**, 1529 (1994).
[59]L. Paolasini, C. Vettier, F. De Bergevin, F. Yakhou, D. Mannix, A. Stunault, W. Neubeck *et al.*, Phys. Rev. Lett. **82**, 4719 (1999).
[60]C. Castellani, C. R. Natoli, and J. Ranninger, Phys. Rev. B **18**, 4945 (1978); **18**, 4967 (1978).
[61]R. M. Moon, Phys. Rev. Lett. **25**, 527 (1970).
[62]M. M. Qazilbash, A. A. Schafgans, K. S. Burch, S. J. Yun, B. G. Chae, B. J. Kim, H. T. Kim, and D. N. Basov, Phys. Rev. B **77**, 115121 (2008).
[63]G. A. Sawatzky and D. Post, Phys. Rev. B **20**, 1546 (1979).